Inverse Problems in Science and Engineering
Vol. 00, No. 00, 00 00, 1–23

Optimal measurement selection for piezoelectric material tensor identification

T. Lahmer, Department of Sensor Technology, University of Erlangen, Germany,
B. Kaltenbacher, Department of Mathematics, University of Stuttgart, Germany,
V. Schulz, Department of Mathematics, University of Trier, Germany

(August 2006)

In this paper we deal with the problem of identifying piezoelectric material parameters from indirect measurements of arbitrarily shaped probes. For this purpose, it is essential to choose the measurement points - i.e., the frequencies where the electrical impedance (and mechanical displacement) data are taken - in an optimal way to maintain reliability on one hand and minimize computational effort on the other hand. For achieving this aim, we develop a method based on ideas from optimum experiment design: Considering cost functions derived from the variance-covariance matrix of the inverse problem, we combine optimal weighting of data points with shifting measurements to optimal positions. Numerical tests illustrate applicability of the proposed methodology.

1 Introduction

Piezoelectric transducers that convert electrical into mechanical energy and vice versa are used in a wide range of applications from injection valves in automotive industry to ultrasound transducers in medical imaging and therapy. Their simulation via a PDE model requires knowledge of certain material tensors, which are hard or even impossible to obtain from direct measurements at the required accuracy [8], [14].

Numerical identification of the material tensors is in principle possible [9], but so far lacks a measure of reliability such as tight confidence intervals around the computed material parameter values. It is the aim of this paper to provide and improve such bounds by means of methods from optimum experiment design [3], [4], [5], [7], [11], [12], [16], [19], [20] and [21].

More concretely, from an application point of view, the use of measurement optimization in the context of piezoelectric material parameter identification is, e.g., motivated as follows: In the course of the production of piezoelectric transducer elements such as stack actuators or piezoelectric discs, the material properties are subject to changes due to variations in the processing conditions. To check quality, measurements of the impedance curves [15], Chapter 9, are made for each produced piece. An improved way of checking will combine

these measurements with an automatic reconstruction of the material parameter set (or at least the subset of relevant parameters). This computational reconstruction has to be both reliable and fast in order not to cause a delay in production time. For this purpose it is necessary to choose optimal measurement frequencies that lead to minimal confidence intervals for the identified material parameters. This optimization is done once and for all before the beginning of the batch production of some transducer element type, while the parameter reconstruction from measurements at the optimized frequencies has to be done very often, namely for each produced piece. Here, the number of measurements n_{meas} decisively influences the computation time in the parameter identification for each produced piece, and therefore should be as small as possible, i.e., equal to or just slightly larger than the number of parameters n_{par} to be reconstructed.

The optimization process suggested in this paper is divided into two parts: In the first part, we start with a large number of possible measurement frequencies, which for obvious reasons leads to the best reliability but requires too time consuming computations for identification. Using a linearization strategy based on weight functions and a variable number of measurement frequencies, by minimization of the confidence interval widths we select n_{meas} frequencies as initial values for the second part of the optimization. Here, the number n_{meas} is only slightly larger than the number n_{par} of searched for material tensor entries. In this second part, the number of frequencies is kept fixed to n_{meas} and the confidence intervals are minimized with respect to the position of the measurement frequencies. This leads to a highly nonlinear optimization problem, for which we can expect convergence only close to a solution. For this reason the first part of initial value construction is really essential. Note that the minimization of confidence intervals at the same time improves the condition of the identification problem. Therefore, and due to the small number of selected frequencies, the second part can be expected to exhibit fast local convergence.

The remainder of this paper is organized as follows: Section 2 describes the piezoelectric PDEs containing the searched for parameters as coefficients. In Section 3 we formulate the inverse problem of piezoelectric material tensor determination, i.e., of coefficient identification in the piezoelectric PDEs. The main emphasis lies on Section 4 where we deal with the problem of selecting the measurement frequencies in our identification process in an optimal way. Finally, in Section 5 we show some numerical results and in Section 6 we summarize and draw some conclusions.

2 Direct problem

The piezoelectric PDEs are a system of four partial differential equations for the mechanical displacement $\vec{u}$ and the electric potential ϕ, inside a piezoelectric body $\Omega \subset \mathbb{R}^3$ (see, e.g., Figure 1 for a simple thickness resonator).

$$\rho \frac{\partial^2 \vec{u}}{\partial t^2} - \mathcal{B}^T \Big(\mathbf{c}^E \mathcal{B}\vec{u} + \mathbf{e}^T \mathrm{grad}\phi \Big) = 0 \ \text{ in } \Omega \tag{1}$$

$$-\mathrm{div}\Big(\mathbf{e}\mathcal{B}\vec{u} - \boldsymbol{\varepsilon}^S \mathrm{grad}\phi \Big) = 0 \ \text{ in } \Omega \ , \tag{2}$$

see for example [2], [9], [13]. In case of the 6-mm crystal class which is considered here

$$\mathcal{B} = \begin{pmatrix} \frac{\partial}{\partial x} & . & . & . & \frac{\partial}{\partial z} & \frac{\partial}{\partial y} \\ . & \frac{\partial}{\partial y} & . & \frac{\partial}{\partial z} & . & \frac{\partial}{\partial x} \\ . & . & \frac{\partial}{\partial z} & \frac{\partial}{\partial y} & \frac{\partial}{\partial x} & . \end{pmatrix}^T \quad , \quad \mathbf{c}^E = \begin{pmatrix} c_{11}^E & c_{12}^E & c_{13}^E & . & . & . \\ c_{12}^E & c_{11}^E & c_{13}^E & . & . & . \\ c_{13}^E & c_{13}^E & c_{33}^E & . & . & . \\ . & . & . & c_{44}^E & . & . \\ . & . & . & . & c_{44}^E & . \\ . & . & . & . & . & c_{66}^E \end{pmatrix} ,$$

$$\mathbf{e} = \begin{pmatrix} . & . & . & . & e_{15} & . \\ . & . & . & e_{15} & . & . \\ e_{31} & e_{31} & e_{33} & . & . & . \end{pmatrix} \quad , \quad \boldsymbol{\varepsilon}^S = \begin{pmatrix} \varepsilon_{11}^S & . & . \\ . & \varepsilon_{11}^S & . \\ . & . & \varepsilon_{33}^S \end{pmatrix} . \tag{3}$$

$\mathcal{B}$ is the three dimensional strain-displacement differential operator, $c_{66}^E = \frac{1}{2}(c_{11}^E - c_{12}^E)$ and $\mathbf{c}^E$, $\boldsymbol{\varepsilon}^S$ are positive definite matrices. Considering the usual

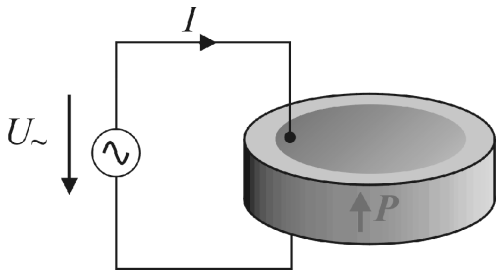

Figure 1. Thickness resonator

experimental setting of vanishing normal stress at the boundary, and two electrodes being attached at opposite positions Γ_g and Γ_e of Ω, one of them loaded with a prescribed voltage ϕ_{load} and the other one grounded, we arrive at the

boundary conditions

$$\begin{aligned} \mathbf{N}^T\sigma &= 0 && \text{on } \partial\Omega \\ \phi &= 0 && \text{on } \Gamma_g \\ \phi &= \phi_{\text{load}} && \text{on } \Gamma_e \\ \vec{n}^T(\mathbf{e}\mathcal{B}\vec{u} - \boldsymbol{\varepsilon}^S\text{grad}\phi) &= 0 && \text{on } \partial\Omega \setminus (\Gamma_g \cup \Gamma_e) \ , \end{aligned} \tag{4}$$

where $\vec{n} = (n_x, n_y, n_z)$ is the outer unit normal vector and

$$\mathbf{N} = \begin{pmatrix} n_x & . & . & . & n_z & n_y \\ . & n_y & . & n_z & . & n_x \\ . & . & n_z & n_y & n_x & . \end{pmatrix}^T ,$$

see Figure 1. Note that we model the electrodes as equipotential surfaces, i.e., $\phi_{\text{load}} = \phi_{\text{load}}(t)$ is independent of the space variable.
We assume sufficient decay as $|t| \to \infty$, so that for each $x \in \Omega$, the field quantities $\vec{u}, \phi$ and their derivatives as appearing in (1), (2) are L^2-functions of time. This is no restriction, since in practice they will have compact support. Thus, we can apply the Fourier transform with respect to the time variable to (1), (2) and obtain the harmonic version of the piezoelectric PDEs

$$-\rho\omega^2\hat{\vec{u}} - \mathcal{B}^T\Big(\mathbf{c}^E\mathcal{B}\hat{\vec{u}} + \mathbf{e}^T\text{grad}\hat{\phi}\Big) = 0 \ \text{ in } \Omega \tag{5}$$

$$-\text{div}\Big(\mathbf{e}\mathcal{B}\hat{\vec{u}} - \boldsymbol{\varepsilon}^S\text{grad}\hat{\phi}\Big) = 0 \ \text{ in } \Omega \ . \tag{6}$$

as well as the same boundary conditions as (4) for the Fourier transformed displacement $\hat{\vec{u}}$ and potential $\hat{\phi}$.
A weak formulation of the boundary value problem (4), (5), (6) (with $\vec{u}, \phi$ replaced by $\hat{\vec{u}}, \hat{\phi}$ in (4)), can be obtained by testing (5) with vector-valued C^∞-functions $\vec{b} = (b_x, b_y, b_z) : \Omega \to \mathbb{C}^3$, and (6) with scalar C^∞-functions w vanishing at the electrodes Γ_g, Γ_e. Integrating by parts

$$\int_\Omega (\mathcal{B}^T\vec{\sigma})^T\overline{\vec{b}}\, d\Omega = -\int_\Omega \vec{\sigma}^T\overline{\mathcal{B}\vec{b}}\, d\Omega + \int_{\partial\Omega} (\mathbf{N}^T\vec{\sigma})^T\overline{\vec{b}}\, d\Gamma \ , \tag{7}$$

we arrive at

$$\begin{aligned} &\hat{\phi}_0(\cdot,\omega) := \hat{\phi}(\cdot,\omega) - \hat{\phi}_{\text{load}}(\omega)\chi(\cdot) \in H^1_{0,\Gamma}(\Omega) \\ &\hat{\vec{u}}(\cdot,\omega) \in H^1_{\mathcal{B}}(\Omega) \end{aligned}$$

For all $\vec{b} \in H^1_{\mathcal{B}}(\Omega)\,, w \in H^1_{0,\Gamma}(\Omega)\ :$

$$\int_\Omega \Big(-\rho\omega^2 \vec{\hat{u}}(\omega)^T \overline{\vec{b}} \ + \ (\mathbf{c}^E \mathcal{B}\vec{\hat{u}}(\omega))^T \overline{\mathcal{B}\vec{b}} \ + \ (\mathbf{e}^T \mathrm{grad}\hat{\phi}_0(\omega))^T \overline{\mathcal{B}\vec{b}} \\ + \ (\mathbf{e}\mathcal{B}\vec{\hat{u}}(\omega))^T \overline{\mathrm{grad} w} \ - \ (\boldsymbol{\varepsilon}^S \mathrm{grad}\hat{\phi}_0(\omega))^T \overline{\mathrm{grad} w} \Big)\, d\Omega$$

$$= \hat{\phi}_{\mathrm{load}}(\omega) \ \int_\Omega \Big(-(\mathbf{e}^T \mathrm{grad}\chi)^T \overline{\mathcal{B}\vec{b}} \ + \ (\boldsymbol{\varepsilon}^S \mathrm{grad}\chi)^T \overline{\mathrm{grad} w} \Big)\, d\Omega\,. \tag{8}$$

Here, $\overline{z}$ denotes the complex conjugate of some $z \in \mathbb{C}$ and the function $\chi \in H^1(\Omega)$ is supposed to be constructed such that $\chi|_{\Gamma_g} \equiv 0 \quad \chi|_{\Gamma_e} \equiv 1\,$; (such a χ exists if Ω is a Lipschitz domain and $\Gamma_e \cap \Gamma_g = \emptyset$). The function spaces

$$H^1_{0,\Gamma} := \overline{\{w \in C^\infty(\Omega) \ : \ w|_{\Gamma_g} = w_{\Gamma_e} = 0\}}^{H^1} \ ,$$

$$H^1_{\mathcal{B}} := \overline{(C^\infty(\Omega))^3}^{H^1_{\mathcal{B}}} \ , \quad ||\vec{b}||_{H^1_{\mathcal{B}}} := ||\vec{b}||_{L^2} + ||\mathcal{B}\vec{b}||_{L^2} \ ,$$

are the closures of the above mentioned test function spaces with respect to appropriate topologies, and to be understood as spaces of complex valued functions. Note that in our situation of imposing Neumann boundary conditions to the mechanical part, Korn's inequality does not apply so that $H^1(\Omega)^3$ is a strict subset of $H^1_{\mathcal{B}}$.

More generally, consider for some $\omega \in R^+$ and

$$\begin{aligned}
&\vec{\hat{f}}_1 \in H^1_{\mathcal{B}}(\Omega))^* \text{ with } \mathcal{N}(\mathcal{B}) \subseteq \mathcal{N}(\vec{\hat{f}}_1(0))\,, \\
&\hat{f}_2 \in H^1_{0,\Gamma}(\Omega))^*\,, \\
&\vec{\hat{g}}_1 \in \left(tr_{\partial\Omega}(H^1_{\mathcal{B}}(\Omega))\right)^*\,, \\
&\hat{\phi}^e \in \mathbb{C}\,, \\
&\hat{g}_2 \in \left(tr_{\partial\Omega\setminus(\Gamma_g \cup \Gamma_e)}(H^1_{0,\Gamma}(\Omega))\right)^*\,,
\end{aligned}$$

where tr_Γ is the trace operator $v \mapsto v|_\Gamma$, to be understood component wise for

vector valued v, the boundary value problem

$$\begin{aligned} -\rho\omega^2\vec{\hat{u}} - \mathcal{B}^T\Big(\mathbf{c}^E\mathcal{B}\vec{\hat{u}} + \mathbf{e}^T\mathrm{grad}\hat{\phi}\Big) &= \vec{\hat{f}}_1 \quad \text{in } \Omega \\ -\mathrm{div}\Big(\mathbf{e}\mathcal{B}\vec{\hat{u}} - \boldsymbol{\varepsilon}^S\mathrm{grad}\hat{\phi}\Big) &= \hat{f}_2 \quad \text{in } \Omega \\ \mathbf{N}^T\Big(\mathbf{c}^E\mathcal{B}\vec{\hat{u}} + \mathbf{e}^T\mathrm{grad}\hat{\phi}\Big) &= \vec{\hat{g}}_1 \quad \text{on } \partial\Omega \\ \hat{\phi} &= 0 \quad \text{on } \Gamma_g \\ \hat{\phi} &= \hat{\phi}^e \quad \text{on } \Gamma_e \\ \vec{n}^T\Big(\mathbf{e}\mathcal{B}\vec{\hat{u}} - \boldsymbol{\varepsilon}^S\mathrm{grad}\hat{\phi}\Big) &= \hat{g}_2 \quad \text{on } \partial\Omega \setminus (\Gamma_g \cup \Gamma_e)\,. \end{aligned} \tag{9}$$

Analogously to Propositions 1, 2 in [9] one sees that for all ω (up to countably many in case of real valued material tensors), there exists a unique and stable weak solution $(\vec{\hat{u}}(\omega), \hat{\phi}(\omega))$. For further well posedness results for the piezoelectric PDEs, we refer to [1], [6], [17], and [18].
In order to solve the piezoelectric PDEs numerically, we use the finite element method, see for example [2], [9], [13].

3 Inverse problem

Our aim is to identify the $n_{\mathrm{par}} = 10$ parameters

$$\begin{aligned} p &= (p_1, p_2, p_3, p_4, p_5, p_6, p_7, p_8, p_9, p_{10})^T \\ &= (c^E_{11}, c^E_{33}, c^E_{12}, c^E_{13}, c^E_{44}, e_{15}, e_{31}, e_{33}, \varepsilon^S_{11}, \varepsilon^S_{33})^T\,, \end{aligned} \tag{10}$$

i.e., the non vanishing entries of $\mathbf{c}^E$, $\mathbf{e}$, $\boldsymbol{\varepsilon}^S$. The given data are electrical and/or mechanical measurements $(\hat{\mathbf{y}}_1, \ldots\ldots, \hat{\mathbf{y}}_{n_{\mathrm{meas}}})$ defined as follows: From impedance measurements [15] one obtains the surface charge $\hat{q}^e$ at the loaded electrode

$$\hat{\mathbf{y}}_i = \hat{q}^e(\omega_i) = \int_{\Gamma_e} \vec{n}^T\Big(-\mathbf{e}\mathcal{B}^T\vec{\hat{u}}(\omega_i) + \boldsymbol{\varepsilon}^S\mathrm{grad}\hat{\phi}(\omega_i)\Big)\,d\Gamma\,, \quad i \in \{1, \ldots, n_{char}\}\,. \tag{11}$$

In addition, one can, for these frequencies, part of them, or even more, measure the mechanical deformation in a boundary point, or rather, its weighted mean value

$$\hat{\mathbf{y}}_{n_{char}+i} = \hat{\overline{u}}(\omega_i) = \frac{1}{|\tilde{\Gamma}|}\int_{\tilde{\Gamma}} S\vec{\hat{u}}(\omega)\;d\Gamma\,, \quad i \in \{1, \ldots, n_{\mathrm{disp}}\}\,. \tag{12}$$

Here, $|\tilde{\Gamma}|$ is the measure of the surface area $\tilde{\Gamma}$ and the matrix S serves as a weight for scaling the mechanical measurements, since these are usually several orders of magnitude smaller in absolute value than the electrical ones.
In sum we therefore have $n_{\text{meas}} = n_{char} + n_{\text{disp}}$ data values $\hat{\mathbf{y}}_j$ by measurements of electrical and/or mechanical quantities at n_{freq} different frequency points.
We denote by $\hat{\mathbf{F}}$ the forward operator mapping the set of parameters to the measurable quantities

$$\begin{aligned} \hat{\mathbf{F}} : \mathbb{C}^{n_{\text{par}}} &\to \mathbb{C}^{n_{\text{meas}}} \\ p &\mapsto \left(\hat{q}_1^e, \ldots, \hat{q}_{n_{char}}^e, \hat{\overline{u}}_1, \ldots, \hat{\overline{u}}_{n_{\text{disp}}}\right)^T , \end{aligned} \tag{13}$$

where $(\hat{\vec{u}}^i, \hat{\phi}^i)$ solves (8) with $\omega := \omega_i$ and $\hat{q}_i^e$, $\hat{\overline{u}}_i$ are derived from $(\hat{\vec{u}}^i, \hat{\phi}^i)$ according to (11), (12). Therewith, we can rewrite the inverse problem under consideration as a nonlinear operator equation

$$\hat{\mathbf{F}}(p) = \hat{\mathbf{y}} \ . \tag{14}$$

This is a finite system of equations for finitely many unknowns. Note, however, that the evaluation of the forward operator involves an infinite dimensional subproblem, namely the solution of (8).
A formulation emphasizing the structure of the forward operator (note that all components of $\hat{\mathbf{F}}$ involve a solution of the same system of PDEs, only the frequencies change) arises from reordering and decomposing $\hat{\mathbf{F}}$ into n_{freq} components $\hat{F}$

$$\hat{F}(p, \omega_i) = \begin{cases} (\hat{q}_i^e, \hat{\overline{u}}_i)^T & \text{if } \hat{q}_i^e \text{ and } \hat{\overline{u}}_i \text{ are measured} \\ \hat{q}_i^e & \text{if only } \hat{q}_i^e \text{ is measured} \\ \hat{\overline{u}}_i & \text{if only } \hat{\overline{u}}_i \text{ is measured.} \end{cases} \tag{15}$$

Equivalently to (14) we get

$$\hat{F}(p; \omega_i) = \hat{y}_i \, , \quad \text{for all } i \in \{1, \ldots, n_{\text{freq}}\} \, ,$$

where the $\hat{y}_i$ denote the respective measured data for the right sides of (15). Given these measurements at fixed frequencies $\omega_1, \ldots, \omega_{n_{\text{freq}}}$, we solve the inverse problem of identifying p by applying Newton type iterations to the operator equation (14), see [9].

4 Optimum experiment design

Our task is to choose the frequency points ω_i, $i = 1, \ldots, n_{\text{freq}}$ where we evaluate measurements in such a way that the sensitivity of the measurements with respect to the searched for material parameters is maximal in the sense that the result of the reconstruction is most robust to errors in the data. For this purpose we assume that the noisy measurements take the form

$$\hat{y}_i^\delta = \hat{y}_i + \varepsilon_i$$

with

$$\varepsilon_i \sim N(0, W_i^{-1}), \quad W_i \in \mathbb{R}_2^2 (\text{or } \mathbb{R}) \text{ symmetric nonnegative definite}$$

so the noise is normally distributed with mean zero and known covariance matrix W_i^{-1} that might also depend on the choice of the frequency points $\boldsymbol{\omega} = (\omega_1, \ldots \omega_{n_{\text{freq}}})$, i.e., $W_i = W(\omega_i)$. We assume for simplicity (and since it in fact realistic) that the noise components are independent of each other. A generalization of the proposed approach to interdependent noise components is straightforward. Here $W(\omega_i)$ is set to $(\delta|\hat{y}_i|)^{-2}$ (to be interpreted as a 2×2 diagonal matrix in case of two measurements at a frequency), where δ is the relative noise level. In our application, we typically have $\delta \sim 0.01$ corresponding to one per cent measurement noise.
We define a solution of the parameter estimation problem with noisy data via a maximum likelihood estimator, i.e., a minimizer of

$$\min_p \frac{1}{2} \sum_{i=1}^{n_{\text{freq}}} \|\hat{F}(p, \omega_i) - \hat{y}_i\|_{W_i}^2 . \tag{16}$$

In this form, we formulate a multi-experiment parameter identification problem, where each ω_i defines an experiment. According to [21] an optimal choice of the frequencies in the above sense then means that we have to minimize some functional φ of the resulting variance-covariance matrix of the parameters

$$\text{Cov}(p, \boldsymbol{\omega}) = (\sum_{i=1}^{n_{\text{freq}}} \hat{F}'(p; \omega_i)^H W(\omega_i) \hat{F}'(p; \omega_i))^{-1} \in \mathbb{C}_{n_{\text{par}}}^{n_{\text{par}}} ,$$

which is hermitian nonnegative definite. Here, $\hat{F}'$ denotes the derivative of the forward operator with respect to the parameters and the superscript H stands for the complex conjugate of its transposed.

4.1 *Fixed number of frequencies*

Let us first consider the situation that we keep the number of frequencies n_{freq} fixed and optimize with respect to the position of the frequencies ω_i.
Using the A-criterion, which minimizes the average variance of the parameters,

$$\varphi(C) = \frac{1}{n_{\text{par}}}\text{trace}(C)\,, \quad C \in \mathbb{R}^{n_{\text{par}}}_{n_{\text{par}}} \tag{17}$$

and assuming the number of measurements as well as the parameter vector to be fixed, we have to solve the minimization problem

$$\min_{\boldsymbol{\omega}} J(\boldsymbol{\omega}) = \min_{\boldsymbol{\omega}} \frac{1}{n_{\text{par}}}\text{trace}\left((\sum_{i=1}^{n_{\text{freq}}} \hat{F}'(p;\omega_i)^H W(\omega_i)\hat{F}'(p;\omega_i))^{-1}\right)\,. \tag{18}$$

Value and gradient of the objective J can be expressed via solutions of systems of the form (9): For given p and $\boldsymbol{\omega}$, we have that the local linearization of $\hat{F}(.;\omega_i)$ in some direction $\underline{dp} \in \mathbb{C}^{n_{\text{par}}}$ is given by

$$\hat{F}'(p;\omega_i)[\underline{dp}] = \begin{cases} (\underline{d\hat{q}}_i, \underline{d\hat{\overline{u}}}_i)^T & \text{if } \hat{q}_i^e \text{ and } \hat{\overline{u}}_i \text{ are measured} \\ \underline{d\hat{q}}_i & \text{if only } \hat{q}_i^e \text{ is measured} \\ \underline{d\hat{\overline{u}}}_i & \text{if only } \hat{\overline{u}}_i \text{ is measured.} \end{cases} \tag{19}$$

for $i \in \{1, \dots n_{\text{freq}}\}$, where the quantities $\underline{d\hat{q}}_i$, $\underline{d\hat{\overline{u}}}_i$ in (19) are determined by (11), (12) from $(\underline{d\vec{\hat{u}}}^{\,i}, \underline{d\hat{\phi}}^i)$ and $(\underline{d\vec{u}}^{\,i}, \underline{d\hat{\phi}}^i)$ solve the variational form of (9) with $\omega = \omega_i$ and

$$\begin{aligned} \vec{\hat{f}}_1 &= \mathcal{B}^T(\underline{d\mathbf{c}}^E\mathcal{B}\vec{\hat{u}}^i + \underline{d\mathbf{e}}^T\text{grad}\hat{\phi}^i) \\ \hat{f}_2 &= \text{div}(\underline{d\mathbf{e}}\mathcal{B}\vec{\hat{u}}^i - \underline{d\varepsilon}^S\text{grad}\hat{\phi}^i) \\ \vec{\hat{g}}_1 &= -\mathbf{N}^T(\underline{d\mathbf{c}}^E\mathcal{B}\vec{\hat{u}}^i + \underline{d\mathbf{e}}^T\text{grad}\hat{\phi}^i)|_{\partial\Omega} \\ \hat{\phi}^e &= 0 \\ \hat{g}_2 &= -\vec{n}^T(\underline{d\mathbf{e}}\mathcal{B}\vec{\hat{u}}^i - \underline{d\varepsilon}^S\text{grad}\hat{\phi}^i)|_{\Omega\setminus(\Gamma_g\cup\Gamma_e)}\,. \end{aligned} \tag{20}$$

Here, $\underline{d\mathbf{c}}^E$, $\underline{d\mathbf{e}}$, $\underline{d\varepsilon}^S$ are the tensors formed from the respective entries in $\underline{dp}$, and $(\vec{\hat{u}}^i, \hat{\phi}^i)$ solve the variational form of the piezoelectric system, i.e., (9) with

$\omega = \omega_i$ and

$$\begin{aligned}
\vec{\hat{f}}_1 &= 0 \\
\hat{f}_2 &= 0 \\
\vec{\hat{g}}_1 &= 0 \\
\hat{\phi}^e &= \hat{\phi}_{\mathrm{load}}(\omega_i) \\
\hat{g}_2 &= 0\,.
\end{aligned}$$

A component of the gradient of J with respect to the frequency vector $\boldsymbol{\omega}$, due to linearity of the trace and by the quotient rule for the derivative of a parameter dependent matrix $C(\lambda)$

$$\frac{\partial}{\partial\lambda}(C(\lambda))^{-1} = -C(\lambda)^{-1}\frac{\partial C}{\partial\lambda}(\lambda)(C(\lambda))^{-1}$$

is given by

$$\frac{\partial}{\partial\omega_i}J(\boldsymbol{\omega}) = -\frac{1}{n_{\mathrm{par}}}\mathrm{trace}\left(\mathrm{Cov}(p,\boldsymbol{\omega})A(p,\boldsymbol{\omega})\mathrm{Cov}(p,\boldsymbol{\omega})\right)\,,$$

where

$$\begin{aligned}
&A(p,\boldsymbol{\omega}) = \\
&\sum_{i=1}^{n_{\mathrm{freq}}}\Big(\hat{F}'_{\omega_i}(p;\omega_i)^H W(\omega_i)\hat{F}'(p;\omega_i) + \hat{F}'(p;\omega_i)^H W(\omega_i)\hat{F}'_{\omega_i}(p;\omega_i) \\
&\qquad\qquad +\hat{F}'(p;\omega_i)^H W_{\omega_i}(\omega_i)\hat{F}'(p;\omega_i)\Big)
\end{aligned}$$

and the subscript $_{\omega_i}$ denotes differentiation with respect to ω_i.

Similarly to (19) one sees that

$$\hat{F}'_{\omega_i}(p;\omega_i)[\underline{dp}] = \begin{cases} (\underline{\Delta\hat{q}}_i, \underline{\Delta\hat{\overline{u}}}_i)^T & \text{if } \hat{q}_i^e \text{ and } \hat{\overline{u}}_i \text{ are measured} \\ \underline{\Delta\hat{q}}_i & \text{if only } \hat{q}_i^e \text{ is measured} \\ \underline{\Delta\hat{\overline{u}}}_i & \text{if only } \hat{\overline{u}}_i \text{ is measured.} \end{cases}$$

where $\underline{\Delta\hat{q}}_i, \underline{\Delta\hat{\overline{u}}}_i$ are determined by (11), (12) from $(\underline{\Delta\vec{\hat{u}}}^{\,i}, \underline{\Delta\hat{\phi}}^i)$ that solve the

variational form of (9) with $\omega = \omega_i$ and

$$\begin{aligned}
\vec{\hat{f}}_1 &= 2\rho\omega_i \underline{d\vec{\hat{u}}}^{\,i} + \mathcal{B}^T(\underline{d\mathbf{c}}^E \mathcal{B}\underline{D\vec{\hat{u}}}^{i} + \underline{d\mathbf{e}}^T \mathrm{grad}\underline{D\hat{\phi}}^{i}) \\
\hat{f}_2 &= \mathrm{div}(\underline{d\mathbf{e}}\mathcal{B}\underline{D\vec{\hat{u}}}^{i} - \underline{d\varepsilon}^S \mathrm{grad}\underline{D\hat{\phi}}^{i}) \\
\vec{\hat{g}}_1 &= -\mathbf{N}^T(\underline{d\mathbf{c}}^E \mathcal{B}\underline{D\vec{\hat{u}}}^{i} + \underline{d\mathbf{e}}^T \mathrm{grad}\underline{D\hat{\phi}}^{i})|_{\partial\Omega} \\
\hat{\phi}^e &= 0 \\
\hat{g}_2 &= -\vec{n}^T(\underline{d\mathbf{e}}\mathcal{B}\underline{D\vec{\hat{u}}}^{i} - \underline{d\varepsilon}^S \mathrm{grad}\underline{D\hat{\phi}}^{i})|_{\Omega\setminus(\Gamma_g\cup\Gamma_e)}\,,
\end{aligned}$$

$(\underline{D\vec{\hat{u}}}^{\,i}, \underline{D\hat{\phi}}^{i})$ solve the variational form of (9) with $\omega = \omega_i$ and

$$\begin{aligned}
\vec{\hat{f}}_1 &= 2\rho\omega_i \vec{\hat{u}}^{i} \\
\hat{f}_2 &= 0 \\
\vec{\hat{g}}_1 &= 0 \\
\hat{\phi}^e &= \hat{\phi}'_{\mathrm{load}}(\omega_i) \\
\hat{g}_2 &= 0\,,
\end{aligned}$$

and $(\underline{d\vec{\hat{u}}}^{\,i}, \underline{d\hat{\phi}}^{i})$, $(\vec{\hat{u}}^{i}, \hat{\phi}^{i})$ are as above. Hence, for evaluating the gradient of the objective J, we have to solve n_{freq} piezoelectric PDE systems (1), (2) with several different right hand sides. Note that this effort cannot be reduced by using an adjoint state approach, since already the state equation itself consists of n_{freq} piezoelectric PDE systems.

Confidence intervals for the parameters can be easily computed from the diagonal entries C_{ii} of the variance-covariance matrix $\mathrm{Cov}(p, \boldsymbol{\omega})$. Namely, with $\chi^2_{n_{\mathrm{par}}}(1-\alpha)$ being the $1-\alpha$ quantile of the $\chi^2_{n_{\mathrm{par}}}$ probability distribution, an approximation to the $100\cdot(1-\alpha)$ per cent confidence region for the parameters is included in the $n_{\mathrm{par}}-$ dimensional box with side lengths $2\sqrt{C_{ii}\chi^2_{n_{\mathrm{par}}}(1-\alpha)}$, see [5]. This means the probability that

$$|p_i^{exact} - p_i^{computed}| \leq \sqrt{C_{ii}\chi^2_{n_{\mathrm{par}}}(1-\alpha)}$$

is larger than $1-\alpha$.

4.2 *Variable number of frequencies*

Better reconstruction results can be expected if not only the values ω_i are to be determined but also their number which could bring in a discrete aspect in the optimization. However, both aspects can be resolved by reformulating the measurement location in the form of a measurement density $\varrho(\omega)$ (not to

be mistaken with the physical mass density ρ appearing in the piezoelectric PDEs (1), (2)), so that the least-squares objective becomes now

$$\min_p \frac{1}{2} \int_{\omega_0}^{\omega_f} \varrho(\omega) \|\hat{F}(p;\omega) - \hat{y}(\omega)\|^2_{W(\omega)} d\omega \tag{21}$$

and the variance-covariance matrix is to be reformulated as

$$\mathrm{Cov}(p) = \left(\int_{\omega_0}^{\omega_f} \varrho(\omega) \hat{F}'(p;\omega)^H W(\omega) \hat{F}'(p;\omega) d\omega \right)^{-1} .$$

We choose $\varrho \in L_1$ with box constraints

$$0 \leq \varrho(\omega) \leq 1 \,. \tag{22}$$

This upper bound 1 may also be increased with the interpretation that at certain frequencies more than one evaluations have to be performed.
Again, using the A-criterion (17) and fixing the parameter vector p, we arrive at the box-constrained minimization problem

$$\min_{0\leq\varrho(\omega)\leq 1} J(\varrho) = \min_{0\leq\varrho(\omega)\leq 1} \frac{1}{n_{\mathrm{par}}} \mathrm{trace} \left(\int_{\omega_0}^{\omega_f} \varrho(\omega) \hat{F}'(p;\omega)^H W(\omega) \hat{F}'(p;\omega) d\omega \right)^{-1} . \tag{23}$$

In order to obtain meaningful results, we should state a maximum number of measurements to be performed, i.e. a maximum total measure of the measurement density as an additional constraint

$$\int_{\omega_0}^{\omega_f} \varrho(\omega) d\omega \leq M \,. \tag{24}$$

The fraction $M/(\omega_f - \omega_0)$ can in the situation of almost continuous measurements be interpreted as the requirement to involve only this fraction of all the available measurement in the least-squares optimization. Experiment design methods based on weight optimization for a discrete set of weights can be found e.g., in [4], [12]. Note that the formulation with a continuous weight function as proposed here is new, to the best of our knowledge. In a numerical implementation, via discretization of the integral it again leads to a finite dimensional optimization problem but gives more freedom for discretizing adaptively instead of fixing the weighted points a priori.
Now the gradient of J with respect to the frequency density ϱ is given by the

following function of $\boldsymbol{\omega}$

$$\frac{\partial}{\partial \varrho} J(\varrho)(\boldsymbol{\omega}) = -\frac{1}{n_{\text{par}}} \text{trace}\left(\text{Cov}(p)\hat{\mathbf{F}}'(p;\boldsymbol{\omega})^H W(\boldsymbol{\omega})\hat{\mathbf{F}}'(p;\boldsymbol{\omega})\text{Cov}(p)\right) .$$

Note that by the introduction of a weight function, the objective in (23) appears to be less nonlinear than in (18).
The integral in the objective has to be approximated by, e.g., summed trapezoidal rule, which gives a natural discretization for ϱ via breakpoints $\omega^{(j)}$, $j \in \{1, \ldots, N\}$ with $N >> n_{\text{par}}$. The derivatives w.r.t. to p have to be computed only once for each $\boldsymbol{\omega}$ value in the discretized problem.
In order to save computational effort in the minimization of the data misfit with respect to the searched for parameters, we neglect frequency points with small weights by thresholding, i.e., given a weight function ϱ, we replace (21) by

$$\min_p \frac{1}{2} \sum_{\omega \in S} \Delta(\omega)\varrho(\omega) \|\hat{F}(p;\omega) - \hat{y}(\omega)\|^2_{W(\omega)} , \tag{25}$$

where

$$S := \{\omega^{(j)} \mid \varrho(\omega^{(j)}) \geq \gamma \max_{\omega} \varrho(\omega)\} := \{\omega^{(j_1)}, \ldots, \omega^{(j_{\text{card}(S)})}\}$$

with $\gamma \in (0,1)$ (typically, $\gamma = 0.8$) and card denoting the cardinality of a set. Moreover,

$$\Delta(\omega^{(j_l)}) := \frac{1}{2}(\omega^{(j_{\min\{l+1,\text{card}(S)\}})} - \omega^{(j_{\max\{l-1,1\}})}) ,$$

so that (25) corresponds to an approximation of the integral in (21) by a composite trapezoidal rule on the (coarse) discretization given by S. If this criterion yields too few frequency points (less than n_{par}), we just select the n_{par} frequency points with the largest weights:

$$\text{if } \text{card}(S) < n_{\text{par}} \text{ set } S := \{\omega^{(j_1)}, \ldots, \omega^{(j_{n_{\text{par}}})}\}$$

where $\max_\omega \varrho(\omega) = \varrho(\omega^{(j_1)}) \geq \varrho(\omega^{(j_2)}) \geq \varrho(\omega^{(j_3)}) \ldots$.
The $100 \cdot (1-\alpha)$ per cent confidence region for the parameters can then be approximated by the $n_{\text{par}}-$ dimensional box with side lengths $2\sqrt{C_{ii}\chi^2_{n_{\text{par}}}(1-\alpha)}$,

where

$$C = \left(\sum_{\omega \in S} \hat{F}'(p;\omega_i)^H W(\omega_i) \hat{F}'(p;\omega_i) \right)^{-1} .$$

Note that the weighting by $\Delta(\omega)\varrho(\omega)$ does not play a role in the size of the confidence intervals, since these obviously have to be invariant with respect to a scaling of the card(S) equations in (14).

A simple iterative scheme for identifying the parameters and optimizing the measurements in a sequential design approach could be

Algorithm 1 Choose $\varrho^0(\boldsymbol{\omega})$, p^1
For $k = 1, 2, 3, \ldots$
Fix $p = p^k$
Solve (23) (or (18)) to obtain ϱ^k (or $\boldsymbol{\omega}^k$)
(e.g. by a projected steepest descent method)
Fix $\varrho = \varrho^k$ (or $\boldsymbol{\omega} = \boldsymbol{\omega}^k$)
Solve (25) (or (16)) to obtain p^{k+1}
(e.g. by a Gauss-Newton iteration with starting value p^k)

Both "Solve" steps can be done in an inexact way with accuracy depending on the state of convergence of the overall method (i.e., large tolerances are used as long as ϱ^k, p^k are "far" from optimal). Note, that here especially in the "Solve (23)" step many forward problems with the same stiffness matrix have to be solved.
Stopping criteria are sufficient smallness of the confidence ellipsoid determined by Cov$(p, \boldsymbol{\omega})$ and/or the changes in ϱ (or $\boldsymbol{\omega}$, respectively) and p.

To arrive at an efficient overall method with large convergence radius, we combine both approaches as follows: The weight function formulation from subsection 4.2 is used for obtaining starting guesses in the highly nonlinear problem of optimizing the positions of a fixed number of frequencies, see subsection 4.1.

4.3 *Descent method*

4.3.1 ***Fixed number of frequencies.*** We define the following sets: $I_m := [\omega_0, \omega_f]$ - the interval in which measurements are available, $I_r := [\omega_r - \epsilon_r, \omega_a + \epsilon_a]$ a set including frequencies between and around frequencies at resonance (ω_r) and antiresonance (ω_a), respectively. The set of admissible frequencies is $I := I_m \setminus I_r$. Here, the constants ϵ_r, ϵ_a are chosen such that measurements are

neither taken between resonance and antiresonance frequency nor very close to them since due to the lack of regularity of the forward problem at eigenfrequencies, the parameter identification method tends to fail in this region. The frequencies ω_r and ω_a are detected just by finding the minimum and maximum of the impedance curve, respectively. Projection onto the feasible set I is done by the operator P defined by $P\omega = \bar{\omega}$ where

$$\tilde{\omega} = \min\{\omega_f, \max\{\omega_0, \omega\}\}$$
$$\bar{\omega} = \omega_c + \text{sign}(\tilde{\omega} - \omega_c)\max\{|\tilde{\omega} - \omega_c|, \tfrac{\omega_r+\epsilon_r-\omega_a+\epsilon_a}{2}\} \quad \text{with } \omega_c = \tfrac{\omega_r+\epsilon_r+\omega_a-\epsilon_a}{2}\,.$$

Since the eigenfrequencies ω_r, ω_a depend on the material parameters, the admissible set I changes in the course of the identification procedure.
The minimization problem

$$\min_{\omega\in I} J(\omega) \tag{26}$$

is numerically solved by the following projected gradient method with line search.

Algorithm 2 Set $\boldsymbol{\omega}^0 \subset I, \lambda^0 > 0, \theta < 1, c_\omega > 0$
While $(||P(\boldsymbol{\omega}^k - \nabla J(\boldsymbol{\omega}^k)) - \boldsymbol{\omega}^k|| > c_\omega)$
$\mathbf{d}^k = -\nabla J(\boldsymbol{\omega}^k)$
While $(J(\boldsymbol{\omega}^k + \lambda^k \mathbf{d}^k) > J(\boldsymbol{\omega}^k))$
$\lambda^k = \theta\lambda^k$
$\boldsymbol{\omega}^{k+1} = \boldsymbol{\omega}^k + \lambda^k \mathbf{d}^k$
$\omega_i^{k+1} = P\omega_i^{k+1} \quad i \in \{1, \ldots, N\},$
$k = k + 1$

4.3.2 ***Variable number of frequencies.*** Also the minimization of (20) is done by a projected gradient method, where P is the projection on the convex feasible set defined by (22), (24) as well as the exception of frequencies too close to resonance and antiresonance, to avoid stability problems in the forward solution.

Algorithm 3 Set $\varrho^0 \in [0,1], \lambda^0 > 0, \theta < 1, \gamma = 0.8, c_\varrho > 0$
While $(||P(\varrho^k - \frac{\partial}{\partial\varrho}J(\varrho^k)) - \varrho^k|| > c_\varrho)$
$\mathbf{d}^k = -\frac{\partial}{\partial\varrho}J(\varrho^k)$
While $(J(\varrho^k + \lambda^k \mathbf{d}^k) > J(\varrho^k))$
$\lambda^k = \theta\lambda^k$
$\varrho^{k+1} = \varrho^k + \lambda^k \mathbf{d}^k$

$\varrho = P\varrho$
Select $S = \{i \in \{1, \ldots, N\} \mid \varrho(\omega^{(i)})^{k+1} > \gamma \max_j \varrho(\omega^{(j)})^{k+1}\}$,
Set $\varrho(\omega^{(i)})^{k+1} = 0$ for $i \notin S$
$k = k + 1$

As an initial guess we use a constant weight function $\varrho^0(\omega) \equiv 0.01$.

5 Numerical results

Our numerical tests were done with simulated data for a piezoelectric disc as in Figure 1 with a radius of 10 mm and a thickness of 1 mm, see Figure 2 for the influence of the probe thickness on the impedance curve. Due to the rotational symmetry, the parameter c_{12}^E has no influence on the transducer behavior [9], hence we identify the nine parameters c_{11}^E, c_{33}^E, c_{13}^E, c_{44}^E, e_{15}, e_{31}, e_{33}, ε_{11}^S, ε_{33}^S here.

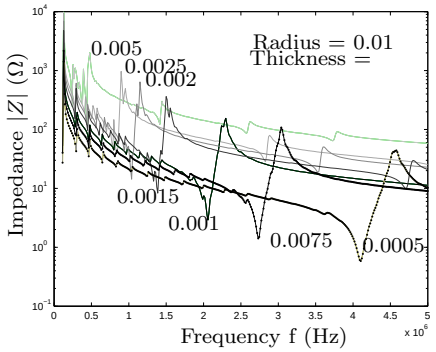

Figure 2. Impedance curves for different thicknesses (actually used: 0.01) for comparison (dashed).

For such a thin disc — a typical thickness resonator — it is easy to obtain nice results for c_{33}^E, e_{33}, ε_{33}^S, but hard to get reliable values for the rest of the parameter set, that can get relevant e.g., as soon as the transducer is operated at lower frequencies close to the radial mode, though. The material under consideration was Pz27, for which we had material parameters from data sheets as well as measurements that had been carried out at the department of sensor technology in Erlangen. All computations were carried out with one per cent normally distributed random noise, and 99 per cent confidence intervals are displayed. For more details about discretization and solution of the forward problem, we refer to [9]. To simulate an industrially relevant scenario, we consider easy to obtain impedance measurements only and do not assume mechanical displacement measurements to be available here.

5.1 *Variable number of frequencies*

For the setting with variable number of frequencies, where we have to optimize the weight function ϱ, we used a discretization of ϱ with thirty equidistant frequency points. As mentioned above, frequency points between and too close to the resonance and antiresonance frequencies are excepted from the range of admissible values. On the other hand, from the identification procedure according to the IEEE standard [8] that is based on resonance frequency measurements, it is clear that the sensitivity for the identification problem is high close to these eigenfrequencies. Therefore the algorithm shifts some of the measurements frequencies as close as possible to the resonance/antiresonance frequency.

In the setting with variable frequency number, we follow two approaches:
Firstly, we apply Algorithm *1* to (23), i.e., we carry out a full optimization of the frequencies by alternating between weight function optimization and parameter fitting. This is computationally quite costly, since parameter fitting has to be done on a fine grid (here: 30 frequency points). The results are displayed in Figures 3, 4, 5.

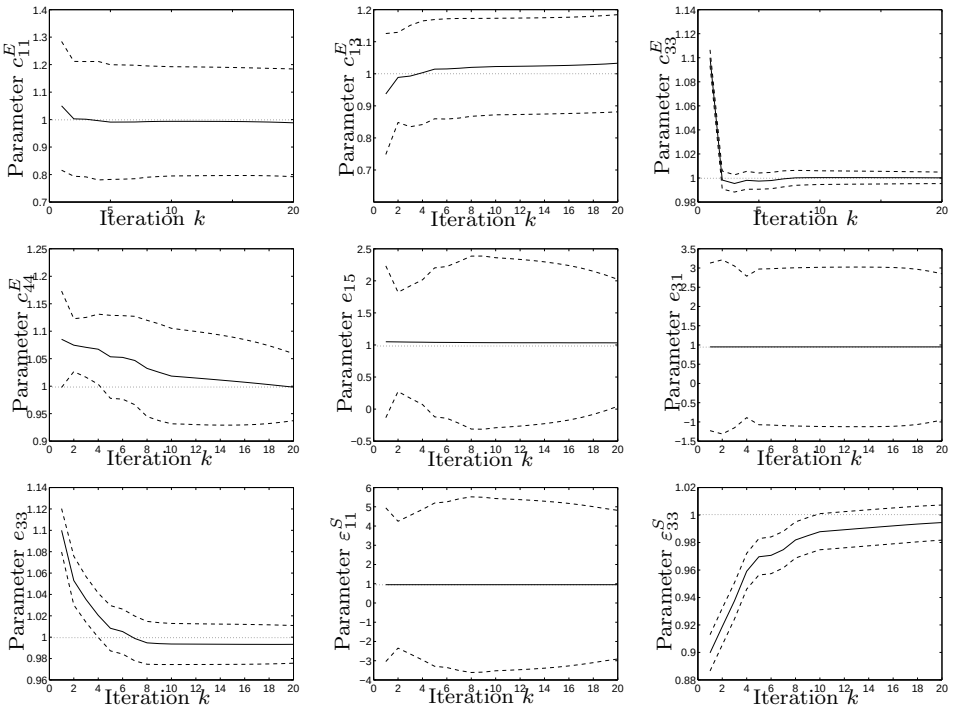

Figure 3. Development of confidence intervals (dashed lines) of the different parameters (solid line) during Algorithm *1* applied to (23).

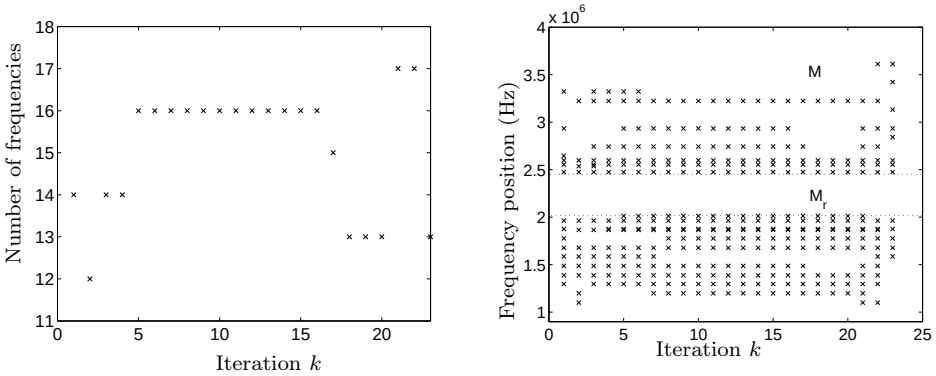

Figure 4. Number (left) and positions (right) of the selected frequencies in each step of Algorithm *1* applied to (23).

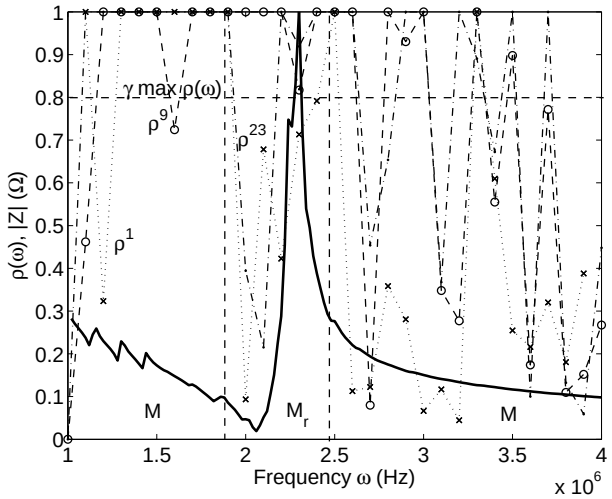

Figure 5. 1st (dotted), 9th (dashed), and 23rd (dash-dotted) iterate of weight function, and impedance curve (solid) for comparison.

The second approach within optimization of a variable number of frequencies is only supposed to generate good starting values for the optimization of the position of a fixed number of frequency values (see Subsection 5.2 below). For this purpose, we only apply one step of the weight function optimization to the initial guess for our parameters, see Figure 6. After this weight function optimization, the frequency points with weights above 80 per cent of the maximal weight (or, if these are too few, those twelve with highest weight,) were selected for parameter fitting. For efficiency reasons, this second approach turns

out to be favorable to the first one in our context.

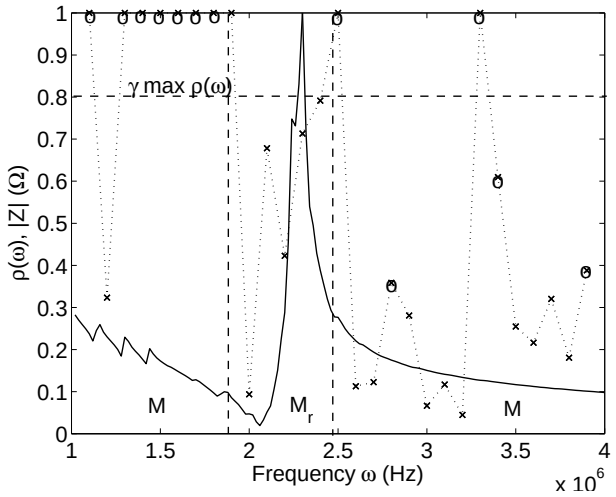

Figure 6. Weight function ϱ (dotted) as well as selected frequencies (o) after one optimization step, and impedance curve (solid) for comparison.

In Figure 7, we plot the resulting confidence intervals of all nine relevant material parameters, compared to those obtained without an optimization of measurement location.

5.2 *Fixed number of frequencies*

After a preprocessing step of determining good approximations for the number and positions of the measurement points, (e.g., by one weight function optimization step, see Subsection 5.1 above), we consider the case described in Subsection 4.1, where we keep the number of frequencies fixed to twelve while optimizing their location.
Figure 8 shows results for the simultaneous identification of all nine relevant material parameters. The narrow intervals for c_{33}^E, e_{33}, and ε_{33}^S reveal the dominant behavior of these parameters for a thickness resonator. Due to the trade-off between all material parameters that is made by the A-criterion, some of the confidence intervals are still too large, see, e.g. ε_{11}^S. Therefore we also consider optimization of the measurement frequencies with respect to single material parameters or subsets of them. Figure 9 shows the (now more satisfactory) result for ε_{11}^S alone, in Figure 10 we plot the results from simultaneous optimization for c_{13}^E, e_{15}, e_{31}, ε_{11}^S.

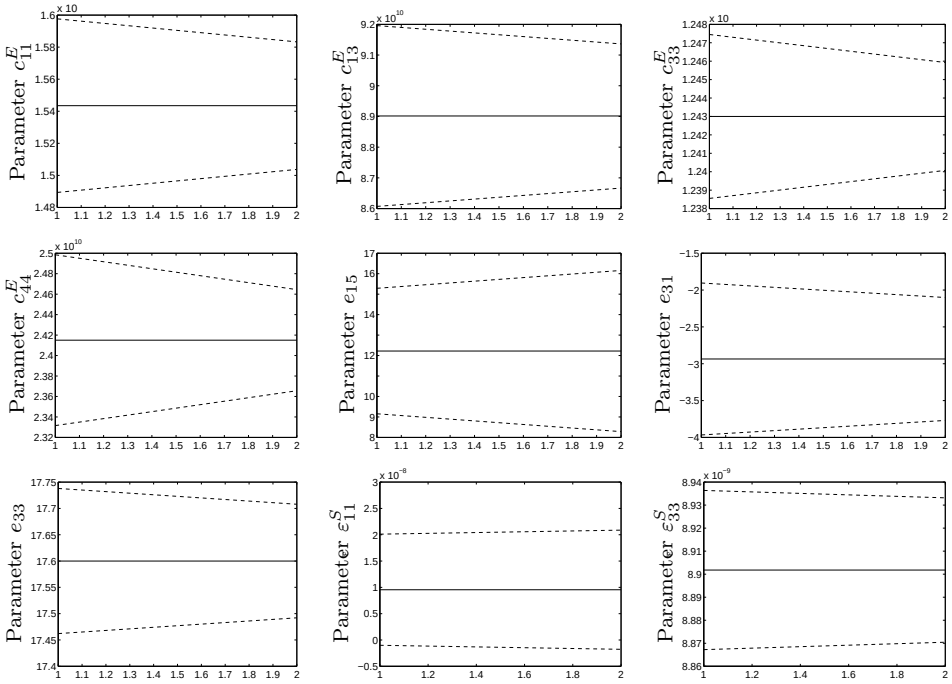

Figure 7. Comparison of confidence intervals: For twelve equidistant frequencies at abscissa value 1, and for the frequencies chosen as in Figure 6 at abscissa value 2.

6 Conclusions and Remarks

For the optimal choice of measurement frequencies in the identification of piezoelectric material parameters, we applied methods of optimum experiment design, that minimize a functional of the variance-covariance matrix of the (linearized) inverse problem. It turned out that a combination of finding starting values via a data weighting approach for variable number of frequencies with a locally convergent gradient method for the highly nonlinear problem of optimal measurement location for fixed number of measurements leads to an efficient optimization scheme.

Further research in this context will be focused on optimal measurement selection for the identification of nonlinear material properties as occurring for large excitations [10].

Moreover, we plan to apply the proposed methodology to material parameter identification problems in different physical contexts such as magnetics, acoustics, or mechanics.

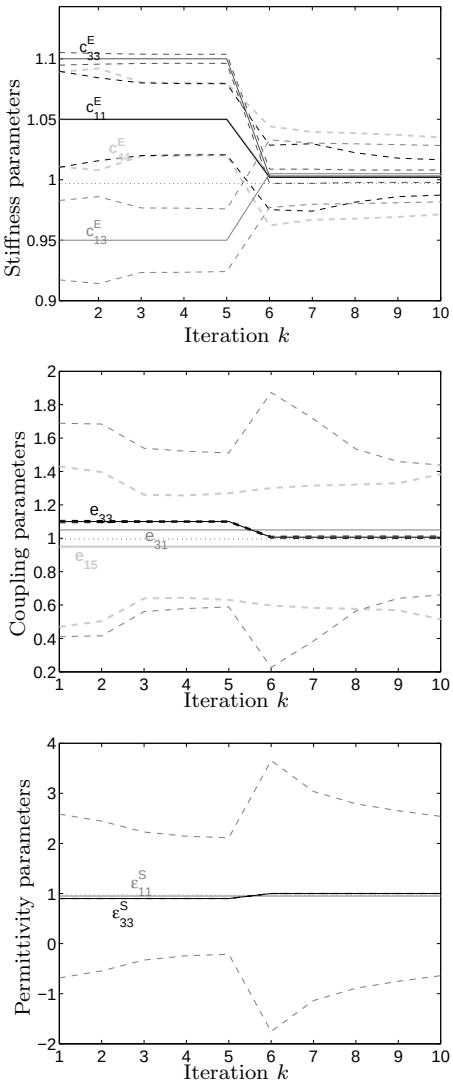

Figure 8. Development of normed values and confidence intervals for all nine material parameters during Algorithm *1* for (18).

Acknowledgment

The authors gratefully acknowledge the fruitful remarks by the referees on a first version of this paper as well as the support by the German Science Foundation DFG under grant Ka/1778-1.

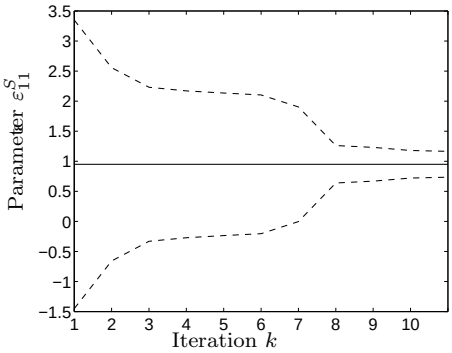

Figure 9. Development of normed values and confidence intervals for one parameter during Algorithm *1* for (18).

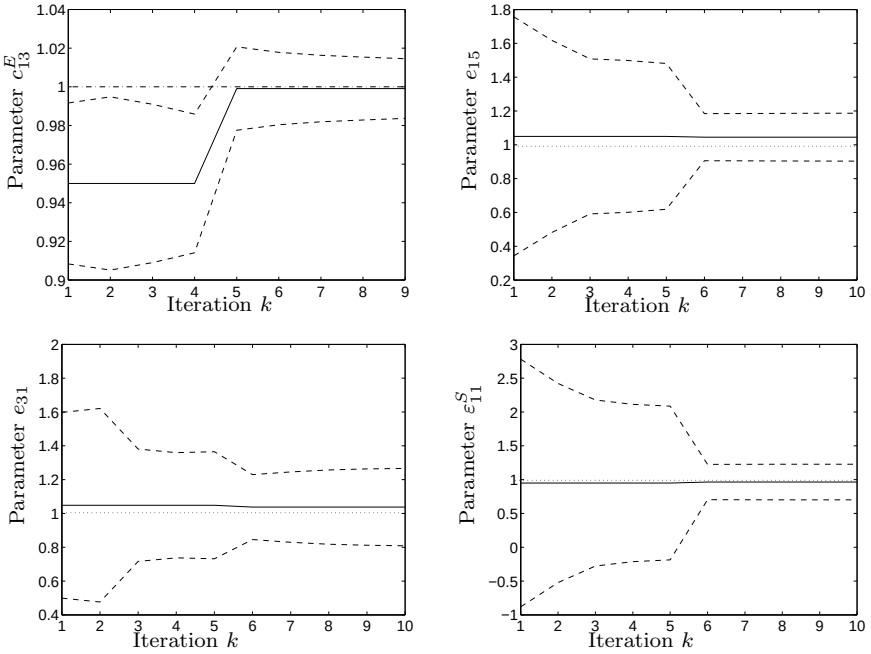

Figure 10. Development of normed values and confidence intervals for four parameters during Algorithm *1* for (18).

References

[1] M. Akamatsu, G. Nakamura, Well-posedness of initial-boundary value problems for piezoelectric equations, *Applicable Analysis,* 81 (2002), 129–141.

[2] H. Allik, T.J.R. Hughes, Finite element methods for piezoelectric vibration, *Int. J. Numer. Meth. Eng.* 2 (1970), 151-157.

[3] A.C. Atkinson, A.N. Donev, *Optimum Experimental Designs*, Clarendon Press, Oxford, 1992.

[4] I. Bauer, H.G. Bock, S. Körkel, J.P. Schlöder, Numerical Methods for Optimum Experimental Design in DAE Systems, *Journal of Computational and Applied Mathematics* 120 (2000), No. 1-2, special issue on SQP-based direct discretization methods for practical optimal control problems (guest-editor: V. Schulz), pp. 1-25.

[5] H.-G. Bock, Randwertproblemmethoden zur Parameteridentifizierung in Systemen nichtlinearer Differentialgleichungen, *Bonner Mathematische Schriften* 183, Bonn, 1987.

[6] W. Geis, G. Mishuris, A.-M. Sändig, Piezoelectricity in multilayer actuators. Modelling and analysis in two and three dimensions, Technical report, University of Stuttgart, 2003.

[7] I. Gherman, V. Schulz, J.T. Betts, Optimal flight trajectories for the validation of aerodynamic models, *Optimization Methods and Software*, 2006 (to appear).

[8] IEEE-UFFC, IEEE Standard on Piezoelectricity, 1985.

[9] B. Kaltenbacher, T. Lahmer, M. Mohr, M. Kaltenbacher, PDE based determination of piezoelectric material tensors, *Eur. J. Appl. Math.* 17 (2006).

[10] B. Kaltenbacher, Determination of parameters in nonlinear hyperbolic PDEs via a multiharmonic formulation, applied in piezoelectric material characterization, *Math. Meth. Mod. Appl. Sci. (M^3AS)*, 16 (2006), 869-895.

[11] J. P. Kaipio, A. Seppänen, E. Somersalo and H. Haario, Posterior covariance related optimal current patterns in electrical impedance tomography *Inverse Problems*, 20 (2004), 919-936

[12] S. Körkel, E. Kostina, Numerical Methods for Nonlinear Experimental Design, In H. G. Bock, E. Kostina, H. X. Phu and R. Rannacher (eds.), Modeling, Simulation and Optimization of Complex Processes, Proceedings of the International Conference on High Performance Scientific Computing, March 10-14, 2003, Hanoi, Vietnam, Springer, 2004, pp. 255-272.

[13] R. Lerch, Simulation of Piezoelectric devices by two- and three- dimensional finite elements, *IEEE Transactions on Ultrasonics, Ferroelectrics, and Frequency control* 37 (1990), 232-247.

[14] R. Lerch, Verbesserung des Verfahrens zur Bestimmung der elektroelastischen Tensoren von piezokeramischen Materialien, technical report, University of Linz, 1996.

[15] R. Lerch, *Elektrische Messtechnik: Analoge, digitale und computergestützte Verfahren* Springer, 2005.

[16] D. Logashenko, B. Maar, V. Schulz, G. Wittum, Optimal geometrical design of Bingham parameter measurement devices, *International Series of Numerical Mathematics (ISNM)*, Vol. 138 (2001), pp. 167-183.

[17] D. Mercier and S.Nicaise, Existence, uniqueness and regularity results for piezoelectric systems, *SIAM J. Math. Anal.* 37 (2005), 651-672.

[18] B. Miara, Controlabilité d'un corps piézoelectrique, *C.R. Acad. Sci. Paris*, 333 (2001), 267–270.

[19] F. Pukelsheim, *Optimal Design of Experiments*, Wiley, New York, 1993.

[20] D. Ucinski, *Optimal Measurement Methods for Distributed Parameter System Identification*, Taylor & Francis, 2004.

[21] V. Schulz, *Compact Course: Nonlinear Optimization and Inverse Problems*, lecture notes for a course held at the University of Stuttgart, March 9-11, 2005.